

Towards Defending Multiple ℓ_p -norm Bounded Adversarial Perturbations via Gated Batch Normalization

Aishan Liu¹, Shiyu Tang¹, Xinyun Chen², Lei Huang¹, Haotong Qin¹, Xianglong Liu^{1*}
and Dacheng Tao^{3,4}

¹Beihang University, Beijing, China.

²Google Brain, Mountain View, USA.

³JD Explore Academy, Beijing, China.

⁴The University of Sydney, Sydney, Australia.

*Corresponding author(s). E-mail(s): xliu@buaa.edu.cn;

Contributing authors: liuaishan@buaa.edu.cn; sytang@buaa.edu.cn; xinyunchen@google.com;
huangleiai@buaa.edu.cn; qinhaotong@buaa.edu.cn; taocheng.tao@gmail.com;

Abstract

There has been extensive evidence demonstrating that deep neural networks are vulnerable to adversarial examples, which motivates the development of defenses against adversarial attacks. Existing adversarial defenses typically improve model robustness against individual specific perturbation types (*e.g.*, ℓ_∞ -norm bounded adversarial examples). However, adversaries are likely to generate multiple types of perturbations in practice (*e.g.*, ℓ_1 , ℓ_2 , and ℓ_∞ perturbations). Some recent methods improve model robustness against adversarial attacks in multiple ℓ_p balls, but their performance against each perturbation type is still far from satisfactory. In this paper, we observe that different ℓ_p bounded adversarial perturbations induce different statistical properties that can be separated and characterized by the statistics of Batch Normalization (BN). We thus propose Gated Batch Normalization (GBN) to adversarially train a perturbation-invariant predictor for defending multiple ℓ_p bounded adversarial perturbations. GBN consists of a multi-branch BN layer and a gated sub-network. Each BN branch in GBN is in charge of one perturbation type to ensure that the normalized output is aligned towards learning perturbation-invariant representation. Meanwhile, the gated sub-network is designed to separate inputs added with different perturbation types. We perform an extensive evaluation of our approach on commonly-used dataset including MNIST, CIFAR-10, and Tiny-ImageNet, and demonstrate that GBN outperforms previous defense proposals against multiple perturbation types (*i.e.*, ℓ_1 , ℓ_2 , and ℓ_∞ perturbations) by large margins.

Keywords: Adversarial defense, multiple perturbation types, batch normalization, model robustness

1 Introduction

Deep neural networks (DNNs) have achieved significant progress across a wide area of applications [1–3]. However, they are susceptible to *adversarial examples* [4, 5]. These attacks are generated by adding human-imperceptible perturbations (often measured

by ℓ_p -norms such as ℓ_1 , ℓ_2 , and ℓ_∞), which could easily mislead DNNs to wrong predictions leading to potential safety threats [6–8].

To improve model robustness against adversarial perturbations, a long line of *adversarial defense* methods have been proposed [5, 9–11]. Currently, most

adversarial defenses are designed to counteract a single type of perturbation (e.g., small ℓ_∞ -norm bounded noise) [12–14]. These defenses offer no guarantees for other ℓ_p -norm adversarial perturbations (e.g., ℓ_1 , ℓ_2), and sometimes even increase model vulnerability to them [15, 16]. However, adversaries are not designated to generate individual-specific perturbation types and are likely to create multiple perturbations to attack the victim model in practice. To address this problem, other adversarial defense strategies have been proposed, with the goal of simultaneously achieving robustness against multiple ℓ_p bounded attacks, i.e., ℓ_∞ , ℓ_1 , and ℓ_2 attacks [16, 17]. Although these methods improve overall model robustness against adversarial attacks in multiple ℓ_p balls, the performance for each individual perturbation type is still far from satisfactory.

In this work, we focus on improving model robustness against multiple ℓ_p bounded adversarial perturbations (such as ℓ_1 , ℓ_2 , and ℓ_∞ adversarial examples in Figure 1). Our primary observation is that different types of ℓ_p -norm adversarial perturbations induce different batch normalization statistical properties (c.f. Figure 2) and have separable characteristics. This observation implies that different types of ℓ_p -norm adversarial perturbations arise in different domains, which we refer to it as *multi-domain hypothesis*. Through theoretical and empirical studies, we found that by simply adversarial training models using a mixture of perturbation types on a single BN, there inevitably exists a domain gap between the training and testing data, which would cause the performance degeneration on model robustness. We thus propose to defend multiple types of adversarial perturbation by designing a multiple-branch BN layer, where each BN branch is in charge of one corresponding perturbation type (i.e., domain) to ensure the normalized output are aligned towards learning perturbation-invariant (domain-invariant) representation.

One remaining problem is that the model does not know which type of perturbation is added during inference. During inference, the adversary would not tell the model which type of perturbations are generated. Therefore, we simultaneously train a gated sub-network, which aims to separate perturbation types on-the-fly. We combine the multi-branch BN layer and the gated sub-network as a building block for DNNs, referred to as *Gated Batch Normalization* (GBN). GBN improves model robustness by separating perturbation-specific information for different perturbation types, and using BN layer statistics to

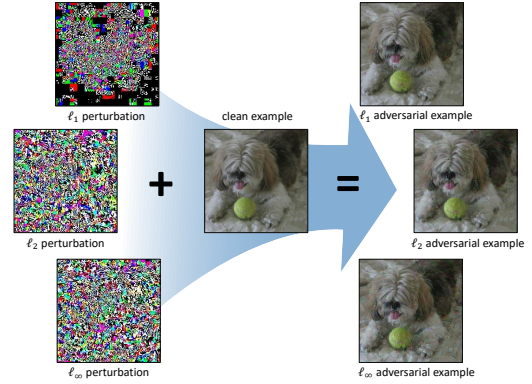


Fig. 1 Visualization of clean examples and corresponding multiple types of adversarial examples (ℓ_1 , ℓ_2 , and ℓ_∞) on ImageNet. These adversarial examples are generated using PGD attacks and the perturbations are constrained by ℓ_1 , ℓ_2 , and ℓ_∞ norm metrics (perturbations are amplified for better visualization).

better align data from the mixture distribution towards perturbation-invariant representations. We conduct extensive experiments on MNIST, CIFAR-10, and Tiny-ImageNet datasets, which demonstrate that our GBN approach outperforms previous defense strategies against multiple adversarial perturbations (i.e., ℓ_1 , ℓ_2 , and ℓ_∞) by large margins, i.e., 10-20%.

Our **contributions** can be summarized as follows:

- We for the first time observe that different types of ℓ_p -norm adversarial perturbations induce different BN statistical properties and arise in different domains, which we refer to it as multi-domain hypothesis.
- Based on our hypothesis, we propose Gated Batch Normalization (GBN) consisting of a multi-branch BN layer and a gated sub-network, to adversarially train an invariant predictor for defending multiple ℓ_p -norm adversarial examples.
- Extensive experiments are conducted to comprehensively evaluate the proposed GBN approach, which demonstrates that our GBN outperforms other baselines against multiple perturbation types by large margins (10-20% absolute improvement).

2 Background and Related work

In this section, we first give the notation in this paper; then we provide a brief overview of existing work on adversarial attacks and defenses, as well as batch normalization techniques.

2.1 Notation

We use the following notation in this paper.

Input space. Let $\mathbb{D} \subset \mathbb{R}^d$ be the input space. Let \mathbf{x} be an input where $\mathbf{x} \in \mathbb{D}$, and $\mathbf{y} \in \mathbb{Y}$ represents the corresponding label for the instance. This paper considers the visual recognition problem and the input space should satisfy $\mathbb{D} = [0, \dots, 255]^d$.

Deep learning model. A DNN f_Θ is a function $\mathbb{D} \rightarrow \mathbb{Y}$ that maps the input space \mathbb{D} to the labels \mathbb{Y} , where Θ denotes the parameters of the model. In this paper, we focus on the image classification task.

Loss function. We use $\ell(f_\Theta(\mathbf{x}), \mathbf{y})$ to denote the loss function for the DNN f_Θ w.r.t. input \mathbf{x} with ground truth label \mathbf{y} . Moreover, we use $\ell(\cdot)$ with subscripts to denote different loss functions in this paper.

Adversarial example. We use $\mathbf{x}_{adv} = \mathbf{x} + \delta$ to denote an adversarial example. The added perturbation δ could make DNNs misclassify the input into wrong labels, i.e., $f_\Theta(\mathbf{x} + \delta) \neq f_\Theta(\mathbf{x})$. Specifically, given a DNN f_Θ and an input image $\mathbf{x} \in \mathbb{D}$ with the ground truth label $\mathbf{y} \in \mathbb{Y}$, an adversarial example \mathbf{x}_{adv} satisfies

$$f_\Theta(\mathbf{x}_{adv}) \neq \mathbf{y} \quad s.t. \quad \|\mathbf{x} - \mathbf{x}_{adv}\| \leq \epsilon, \quad (1)$$

where $\|\cdot\|$ is a distance metric.

Different ℓ_p -norm adversarial examples. From Eqn 1, adversarial attacks can be often categorized based on the types of perturbations measured by different distance metrics $\|\cdot\|$ (e.g., ℓ_p -norms bounded perturbations). In this paper, we primarily consider ℓ_1 , ℓ_2 , and ℓ_∞ adversarial attacks by solving Eqn 1, where the perturbations are measured and constrained by ℓ_1 , ℓ_2 , and ℓ_∞ norms, respectively. In particular, let \mathbb{D}^0 denote the set of clean examples, and \mathbb{D}^k ($k = 1, \dots, N$) denote the set of adversarial examples generated by the k -th adversarial perturbation type. An adversarial example of the k -th type \mathbf{x}_{adv}^k is generated by the pixel-wise addition of the perturbation δ^k , i.e., $\mathbf{x}_{adv}^k = \mathbf{x} + \delta^k$. The perturbations δ^k are measured by different ℓ_p -norms.

2.2 Adversarial attacks

Adversarial examples are perturbed inputs intentionally designed to mislead DNNs [4, 5]. These generated perturbations are human imperceptible, but could easily lead DNNs to wrong predictions.

Extensive studies have been proposed to optimize adversarial perturbations so that they could generate

adversarial examples to attack deep learning models [4, 5, 7, 18–20]. These imperceptible perturbations could easily make DNNs misclassify the input images. Besides adversarial perturbations, adversarial patches are designed to attack DNNs by attaching additional stickers for their feasibility in the physical world [18, 21, 22], including patches [21], camouflages [22], and light [23]. In general, adversarial attacks can be roughly categorized into *white-box* and *black-box* manners. For *white-box* attacks, adversaries have complete knowledge of the target model and can fully access it [5, 12, 24]; for *black-box* attacks, adversaries have limited model knowledge and can not directly access the model [25–29].

2.3 Adversarial defenses

Adversarial defenses aim to improve model robustness against adversarial attacks, which play important roles in increasing the availability of DNNs. In the adversarial machine learning literature, various defense approaches have been proposed to improve model robustness against adversarial examples [9, 12, 30–34]. Among them, adversarial training has been widely studied and demonstrated to be the most effective defense strategy [5, 12, 35]. Specifically, adversarial training minimizes the worst case loss within some perturbation regions for classifiers, by augmenting the training set with adversarial examples. Formally, given a deep neural network f_Θ , training data $\{\mathbf{x}^{(i)}, \mathbf{y}^{(i)}\}_{i=1 \dots n}$, the robust optimization problem is to solve the min-max problem as

$$\min_{\Theta} \sum_i \max_{\delta} \ell(f_\Theta(\mathbf{x}^{(i)} + \delta), \mathbf{y}^{(i)}),$$

where δ is bounded by ℓ_p perturbations with radius ϵ . To solve the inner optimization, the typical solution is addressed by using a form of adversarial attacks [5, 12]. Specifically, adversarial training with PGD attacks, which incorporates adversarial examples generated by PGD attack into training, has so far remained empirically robust [12].

However, these defenses only improve model robustness for specific ℓ_p -norm perturbation (e.g., ℓ_∞) and typically offer no robustness guarantees against other ℓ_p -norm attacks [15, 16, 36]. To address this problem, recent works have attempted to improve the robustness against several types of ℓ_p -norm perturbation. [36] proposed Analysis by Synthesis

(ABS), which used multiple variational autoencoders to defend ℓ_0 , ℓ_2 , and ℓ_∞ adversaries. However, ABS only works on the MNIST dataset. [37] proposed a provable adversarial defense against all ℓ_p norms for $p \geq 1$ using a regularization term. However, it is not applicable to the empirical setting, since it only guarantees robustness for very small perturbations (*e.g.*, 0.1 and $2/255$ for ℓ_2 and ℓ_∞ on CIFAR-10). [16] tried to defend against multiple perturbation types (ℓ_1 , ℓ_2 , and ℓ_∞) by combining different types of adversarial examples for adversarial training. Specifically, they introduced two training strategies, “MAX” and “AVG”, where for each input image, the model is either trained on its strongest adversarial example or all types of perturbations. More recently, [17] proposed multi steepest descent (MSD), and showed that a simple modification to standard PGD adversarial training improves robustness to ℓ_1 , ℓ_2 , and ℓ_∞ adversaries. There also exist another line of work, which focuses on improving model robustness against multiple non- ℓ_p adversarial attacks (*e.g.*, adversarial patches) and unseen perturbations (*e.g.*, corruptions) [15, 38, 39]. In this work, we follow [16, 17] to focus on defense against ℓ_1 , ℓ_2 , and ℓ_∞ adversarial perturbations. In contrast to the previous studies, our paper proposes a different solution as (1) we propose the multi-domain hypothesis and treat different ℓ_p -norm adversarial examples as different data domains for better defense, while previous studies treat them similarly; (2) we propose GBN as a defense solution that first separates different perturbations on-the-fly and then uses different BN branches to normalize them into aligned features, while others directly feed different attacks into models for adversarial training; and (3) we outperform others against multiple perturbation types by large margins (10-20% absolute improvement).

Another concurrent work [40] proposed a two-stage pipeline with multiple models by categorizing the input and then sending them to the corresponding constitute model. Our paper differs from [40] significantly: (1) Motivation. [40] tries to defend multiple perturbations by employing several ℓ_p adversarially-trained models, while our GBN aims to train a (single) perturbation-invariant model for tackling multiple perturbations. (2) Technical implementation. [40] first categorizes input examples and then feeds them to corresponding specialized robust predictors (different ℓ_p adversarially-trained models). In contrast, at each layer of the model, our GBN first uses a gated sub-network to separate the perturbations on-the-fly and

then uses different BN branches to normalize them into aligned features for the learning of subsequent convolutional layers. (3) Usability. Our GBN could be embedded into any networks with batch normalization and can be combined with other defenses, while [40] relies on other adversarially trained models.

2.4 Batch normalization

BN [41] is typically used to stabilize and accelerate DNN training. Besides, a number of normalization techniques have been proposed to improve BN for style-transfer [42], domain adaption [43–46], training of GANs [47], and building efficient DNNs [48]. Let $\mathbf{x} \in \mathbb{R}^d$ denote the input to a neural network layer. During training, BN normalizes each neuron/channel within m mini-batch data by

$$\hat{\mathbf{x}}_j = BN(\mathbf{x}_j) = \gamma_j \frac{\mathbf{x}_j - \mu_j}{\sqrt{\sigma_j^2 + \xi}} + \beta_j, \quad j = 1, 2, \dots, d, \quad (2)$$

where $\mu_j = \frac{1}{m} \sum_{i=1}^m \mathbf{x}_j^{(i)}$ and $\sigma_j^2 = \frac{1}{m} \sum_{i=1}^m (\mathbf{x}_j^{(i)} - \mu_j)^2$ are the mini-batch mean and variance for each neuron, respectively, and ξ is a small number to prevent numerical instability. The learnable parameters γ and β are used to recover the representation capacity. During inference, the population statistics of mean $\hat{\mu}$ and variance $\hat{\sigma}^2$ are used in Eqn. 2, which are usually calculated as the running average over different training iterations t with update factor α :

$$\begin{cases} \hat{\mu}^t = (1 - \alpha)\hat{\mu}^{(t-1)} + \alpha\mu^{t-1}, \\ (\hat{\sigma}^t)^2 = (1 - \alpha)(\hat{\sigma}^{(t-1)})^2 + \alpha(\sigma^{(t-1)})^2. \end{cases} \quad (3)$$

For the convolutional input $\mathbf{X} \in \mathbb{R}^{d \times h \times w}$, where h and w are the height and width of the feature map, BN jointly normalize all the activations in a batch, over all locations [41]. That is, the normalization operation in Eqn. 2 is performed within the effective mini-batch of size mhw .

We will provide comparisons of our GBN and other normalization methods in Section 3.5 and 4.2.

3 Gated Batch Normalization

In this section, we first provide the problem definition, and then briefly illustrate our multi-domain hypothesis, which states that different ℓ_p bounded adversarial

examples are drawn from different domains. Motivated by that, we propose Gated Batch Normalization (GBN), which improves model robustness against multiple adversarial perturbations.

3.1 Problem Definition

Goal. For an image classification model, given input image \mathbf{x} , a model f_{Θ} is designed to predict the ground truth label \mathbf{y} by solving the following problem:

$$\min_{\Theta} \sum_{i=1}^n \ell(f_{\Theta}(\mathbf{x}^{(i)}, \mathbf{y}^{(i)})), \quad (4)$$

where n denotes the number of input samples.

The purpose of our proposed GBN approach is to defend against multiple ℓ_p -norm adversarial perturbations, *i.e.*, provide correct predictions given adversarially perturbed inputs as

$$\min_{\Theta} \sum_{i=1}^n \sum_{k=1}^N \ell(f_{\Theta}(\mathbf{x}^{(i)} + \delta^k, \mathbf{y}^{(i)})), \quad (5)$$

where n denotes the number of input samples, and N represents perturbation type numbers. Formally, we aim to build robust DNNs through adversarial training scheme by solving the min-max optimization as

$$\min_{\Theta} \sum_{i=1}^n \sum_{k=1}^N \max_{\delta^k} \ell(f_{\Theta}(\mathbf{x}^{(i)} + \delta^k, \mathbf{y}^{(i)})). \quad (6)$$

Threat model. In this paper, we consider the two commonly-adopted scenarios and assumptions, *i.e.*, white-box and black-box. We first consider the basic *white-box* threat model, where adversaries have direct access to the model including architecture and parameters. Meanwhile, we also assume that adversaries do not have access to the model, and need to perform *black-box* attacks. Our defense aims to provide model robustness against multiple ℓ_p -norm adversarial examples in both white-box and black-box scenarios. To verify our defense ability, for white-box assumption, we employ commonly-used gradient-based attacks (*c.f.* Section 4.2) and adaptive attacks that are specially designed to break our GBN block (*c.f.* Section 4.3); for black-box assumption, we adopt several gradient-free and black-box attacks (*c.f.* Section 4.2).

3.2 Motivation: Multi-domain hypothesis

We assume N *adversarial perturbation types*¹, each characterized by a set \mathbb{S}^k of perturbations for input \mathbf{x} . Our hypothesis states that different ℓ_p norm bounded adversarial perturbations \mathbb{D}^k (for all $k \geq 0$, including clean examples) are drawn from different domains.

We first empirically verify the hypothesis by training a DNN with each BN layer composed of several BN branches. Specifically, we train a DNN on CIFAR-10 with each BN layer composed of 4 branches (*i.e.*, we replace each BN with 4 BN branches, the structure multiple BN branches is shown in Figure 2(a)). During training, we construct different mini-batches for clean, ℓ_1 , ℓ_2 , and ℓ_{∞} adversarial images (*i.e.*, \mathbb{D}^0 , \mathbb{D}^1 , \mathbb{D}^2 , and \mathbb{D}^3) to estimate the normalization statistics of each branch of BN; during inference, given a mini-batch of data from a specific domain, we manually activate the corresponding BN branch and deactivate the others. We update the running statistics of each BN branch separately but optimize the model parameters using the sum of the four losses (*i.e.*, clean, ℓ_1 , ℓ_2 , and ℓ_{∞} adversarial examples). The results in Figure 2(b) have shown that different \mathbb{D}^k induce significantly different running statistics, according to the different running means and variances. More studies including running statistics results and Fourier analysis can be found in Section 5.1. Thus, training on a single perturbation type (domain) is insufficient for achieving the robustness against other types of perturbations (domains).

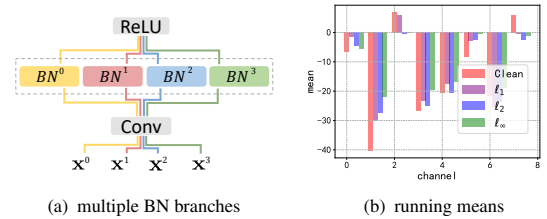


Fig. 2 (a): the structure with 4 BN branches, which use different mini-batches from different \mathbb{D}^k to estimate the normalization statistics. (b): running means of multiple BN branches on 8 randomly sampled channels in a VGG-16's *conv2_1* layer.

Based on the above analysis, an intuitive solution is to training on a mixture of different perturbation types. However, during inference, adversaries are likely to generate different perturbation types with different ratios. According to our Theorem 1 (*c.f.* *proof*

¹In this work, we consider $N = 3$ adversarial perturbation types: ℓ_1 , ℓ_2 , and ℓ_{∞} .

in supplementary material), by training with a mixture of perturbation types on a single BN, there inevitably exists a domain gap between training and testing data, which causes the performance degeneration [49].

Theorem 1 For a specific batch normalization layer, the corresponding input feature set of the dataset with N adversarial perturbation types can be expressed as $\mathbb{F} = (\mathbb{F}_1, \dots, \mathbb{F}_N)$. When we assume that the feature \mathbb{F}_k (generated k -th type data in feature) inputted to the batch normalization layer follows a Gaussian distribution $\mathcal{N}(\mu_k, \sigma_k)$ and the sampling probability of \mathbb{F} is \mathbf{w} ; $\|\mathbf{w}\|_{\ell_1} = 1$ and $\mathbf{w}' = \mathbf{w} + \mathbf{e}_w$; $\|\mathbf{w}'\|_{\ell_1} = 1$ in two different sets \mathbb{S}_1 and \mathbb{S}_2 , respectively, the difference of the mixture distribution statistics between \mathbb{S}_1 and \mathbb{S}_2 can be expressed as $\Delta_\mu = \mathbf{e}_w \boldsymbol{\mu}^T$ and $\Delta_\sigma = \mathbf{e}_w \mathbf{t}^T - 2(\mathbf{w} \boldsymbol{\mu}^T)(\mathbf{e}_w \boldsymbol{\mu}^T) - (\mathbf{e}_w \boldsymbol{\mu}^T)^2$, where $\boldsymbol{\mu} = (\mu_1, \dots, \mu_k)$ and $\mathbf{t} = (\mu_1^2 + \sigma_1^2, \dots, \mu_k^2 + \sigma_k^2)$, $\Delta_\mu = 0$ and $\Delta_\sigma = 0 \iff \mathbf{e}_w = \mathbf{0}$.

To verify this, we train several individual models with different ratios of perturbation types for the estimation of the single BN layer, and we spot the obvious performance degeneration when the proportion of different perturbations types in the training set is different to that in the test set. This scenario would break the independently identically distribution assumption and make the single BN fail [41]. See Section 5.1 for experimental results.

Thus, instead of learning a mixture distributions with a single BN, we utilize a **multi-branch BN layer, in which each BN branch is in charge of one corresponding perturbation type (i.e., domain)**. Besides, the output of each perturbation is normalized by corresponding BN towards learning domain-invariant representation. One remaining problem is that the model does not know the input domain during inference. Existing work suggested that adversarial examples are separable from clean examples [50], and clean/adversarial examples are drawn from different domains [51]. Therefore, we **introduce a gated sub-network to separate perturbations from different domains during inference, i.e., separates domain-specific (perturbation-specific) information**.

Thus, the multi-domain hypothesis motivates the design of GBN, which consists of a gated sub-network and a multi-branch BN layer.

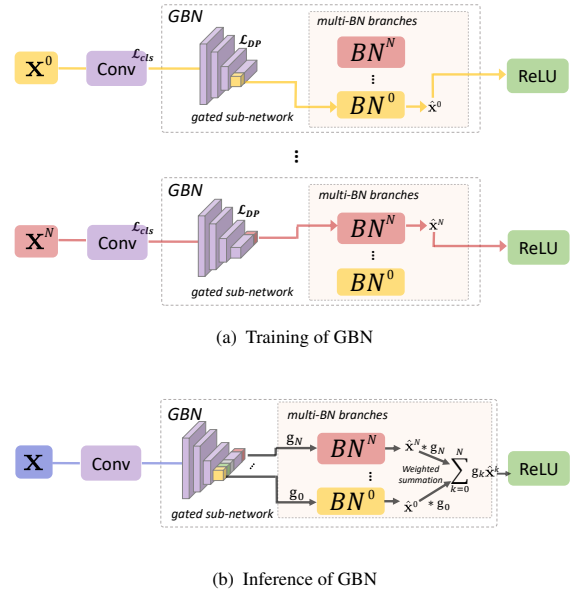


Fig. 3 The training and inference procedures of GBN. During training, samples from different domains (denoted by different colors) are fed into corresponding BN branches to update the running statistics. During inference, the calculation process works in a sequential manner. Given input data from an unknown domain, the gated sub-network first predicts the domain of input \mathbf{x} ; GBN then lets \mathbf{x} go through each BN branch $BN^k(\cdot)$ and obtain the normalized output $\hat{\mathbf{x}}^k$; finally, we jointly normalize the output by calculating a weighted summation as $\sum_{k=0}^N g_k \hat{\mathbf{x}}^k$.

3.3 Gated Batch Normalization architecture

To train a perturbation-invariant predictor and obtain domain-invariant representations for multiple ℓ_p bounded adversarial perturbations, we use the BN layer statistics to align data from the mixture distribution. Specifically, GBN uses a BN layer with multiple branches $\Psi = \{BN^k(\cdot), k = 0, \dots, N\}$ during training, where each branch $BN^k(\cdot)$ is exclusively in charge of the domain \mathbb{D}^k . The aligned data are then aggregated as the input to subsequent layers to train a classifier, which achieves the minimum risk across different domains (i.e., the best robustness to different perturbations with a high accuracy on clean data).

To separate the input domain during inference and calculate the normalized output, GBN utilizes a gated sub-network $\Phi_\theta(\mathbf{x})$ to predict the domain for each layer input \mathbf{x} , and we will illustrate how to train $\Phi_\theta(\mathbf{x})$ in Section 3.4. Given the prediction of sub-network $\mathbf{g} = \Phi_\theta(\mathbf{x})$ that outputs the confidence over $N + 1$ domains, we calculate the normalized output in

a soft-gated way:

$$\hat{\mathbf{x}} = \text{GBN}(\mathbf{x}) = \sum_{k=0}^N \mathbf{g}_k \hat{\mathbf{x}}^k, \quad (7)$$

where \mathbf{g}_k represents the confidence of \mathbf{x} belonging to the k -th domain; $\hat{\mathbf{x}}^k$ is the normalized output of $\text{BN}^k(\cdot)$, which uses the population statistics of the domain \mathbb{D}^k to perform the normalization.

We provide an overview of the inference procedure in Figure 3(b) and Algorithm 1. In the *supplementary material*, we discussed an alternative approach that takes the top-1 prediction of \mathbf{g} (the hard label), and show that our soft-label version achieves slightly better results than the hard-label one.

Our GBN aims to disentangle domain-invariant features and domain-specific features: (1) the distributions of different domains are aligned by their normalized outputs (all are standardized distributions), which ensures that the following linear layers learn domain-invariant representations; and (2) the domain-specific features for each domain \mathbb{D}^k are obtained by the population statistics $\{\hat{\mu}^k, \hat{\sigma}^k\}$ of its corresponding BN branch $\text{BN}^k(\cdot)$.

Algorithm 1 Inference of Gated Batch Normalization

Input: Layer input \mathbf{x}

Output: Normalized output by GBN

- 1: Compute the output of gated sub-network $\mathbf{g} = \Phi_{\theta}(\mathbf{x})$
 - 2: **for** k in $N+1$ domains **do**
 - 3: Let \mathbf{x} go through $\text{BN}^k(\cdot)$ and obtain the normalized output $\hat{\mathbf{x}}^k$ based on Eqn. 2.
 - 4: **end for**
 - 5: Compute GBN output based on Eqn. 7.
-

3.4 Training

We provide an overview of the training procedure in Figure 3(a), and the details are in Algorithm 2. Specifically, for each mini-batch \mathcal{B}^0 consisting of clean samples, we use PGD [12] to generate batches of adversarial examples \mathcal{B}^k ($k \in \{1, \dots, N\}$) for each domain \mathbb{D}^k . To capture the domain-specific statistics of different perturbation types, given the mini-batch data \mathcal{B}^k from domain \mathbb{D}^k , we ensure that \mathcal{B}^k goes through its corresponding BN branch $\text{BN}^k(\cdot)$, and we use Eqn. 2 to compute the normalized output $\hat{\mathcal{B}}^k$. The

population statistics $\{\hat{\mu}^k, \hat{\sigma}^k\}$ of $\text{BN}^k(\cdot)$ are updated based on Eqn. 3. In other words, we disentangle the mixture distribution for normalization and apply separate BN branches to different perturbation types for statistics estimation.

To train the gated sub-network \mathbf{g} , we provide the supervision of the input domain for each training sample. Specifically, we introduce the domain prediction loss \mathcal{L}_{DP} :

$$\mathcal{L}_{DP} = \sum_{k=0}^N \sum_{\mathbf{x} \sim \mathbb{D}^k} \ell(\Phi_{\theta}(\mathbf{x}), k). \quad (8)$$

Finally, we optimize the parameters Θ of the entire neural network (e.g., the weight matrices of the convolutional layers, except for the gated sub-network) using the classification loss \mathcal{L}_{cls} :

$$\mathcal{L}_{cls} = \sum_{k=0}^N \sum_{(\mathbf{x}, \mathbf{y}) \in \mathbb{D}^k} \ell(f_{\Theta}(\mathbf{x}; \text{BN}^k(\cdot)), \mathbf{y}). \quad (9)$$

where $\text{BN}^k(\cdot)$ is the corresponding BN branch.

Algorithm 2 Training of Gated Batch Normalization (GBN) for Each Iteration.

Input: Network f with GBN

Output: Model parameters Θ and θ

- 1: Given the mini-batch data \mathcal{B}^0 , use PGD algorithm to generate batches of adversarial examples \mathcal{B}^k ($k \in \{1, \dots, N\}$) of different perturbation types
 - 2: **for** k in $N+1$ domains **do**
 - 3: Let \mathcal{B}^k go through $\text{BN}^k(\cdot)$ at each layer to obtain normalized outputs $\hat{\mathcal{B}}^k$, using Eqn. 2.
 - 4: Update the population statistics $\{\hat{\mu}^k, \hat{\sigma}^k\}$ of $\text{BN}^k(\cdot)$ at each layer, using Eqn. 3.
 - 5: **end for**
 - 6: Update θ (parameters of the gated sub-network at each layer) based on Eqn. 8.
 - 7: Update Θ (parameters of the whole network) based on Eqn. 9.
-

3.5 Discussion over other normalization techniques

Since our GBN block is based on the batch normalization technique, we further compare the differences between our GBN and other related normalization

techniques including Mode Normalization (MN) [45] and MBN [51, 52].

Our GBN differs from them to a large extent in the following aspects: (1) Goal. The goal of MBN is to improve image recognition or analyze the properties of BN for adversarial training, and MN aims to tackle the problem of multi-task/multi-distribution learning. In contrast, our GBN is the first to defend against adversarial attacks using multiple BNs on adversarially trained models and further generalize to multiple perturbations. (2) Motivation and implementation. For MN, though also containing gated networks, it only adopts two BN branches (without direct correspondence to specific domains) regardless of the domain numbers. In other words, MN aims to learn a mixture distribution for several domains and normalizes the input with different weights from the two mixed distributions. In contrast, our GBN separates domain-specific statistics for different domains (each BN captures the statistics for each domain) and then aligns data to build domain-invariant representations. For MBN, it applies two BNs to clean and adversarial examples for statistics estimation, and manually selects the BN branch for each input image. This is impractical since it requires prior knowledge of the input domain during inference. However, our GBN can predict the domain of input and route the corresponding BN branches during inference. (3) Performance. The experimental results in Table 1 and Section 4.4 verify the effectiveness of our motivation (+20% absolute robustness improvement). In addition, these results indicate that simply normalizing inputs with mixture distribution statistics (MN) or using fixed unrelated statistics (MBN) is less effective for defending multiple types of perturbations.

4 Experiments

We evaluate the effectiveness of our GBN block to simultaneously defend against ℓ_1 , ℓ_2 , and ℓ_∞ perturbations, which are the most representative and commonly used adversarial perturbation types.

4.1 Experimental setup

Datasets. In this paper, we conduct experiments on image classification benchmarks, including MNIST [53], CIFAR-10 [54], and Tiny-ImageNet [55]. MNIST is a dataset containing 10 classes of handwritten digits of size 28×28 ; CIFAR-10 consists of 60,000 natural scene color images in

10 classes of size 32×32 ; Tiny-Imagenet has 200 classes of size 64×64 . For our experiments, we use the given training set in each datasets to train our models, and divide the given test set in each datasets into validation set and test set (the ratio between validation set and test set is 2:8). In each training epoch we use the validation set to validate the performance of the trained models. After finishing training, we use test set to evaluate the final performance of the models.

Architectures and hyperparameters. We use LeNet [56] for MNIST; ResNet-20 [57], VGG-16 [58], and WRN-28-10 [59] for CIFAR-10; and ResNet-34 [57] for Tiny-ImageNet. For fair comparisons, we keep the architecture and main hyperparameters the same for GBN and other baselines. Specifically, all the models for each method on MNIST, CIFAR-10, and Tiny-ImageNet are trained for 40, 40, and 20 epochs, respectively. We set the mini-batch size=64, use the SGD optimizer with weight decay 0.0005 for Tiny-ImageNet and use no weight decay for MNIST and CIFAR-10. We set the learning rate as 0.1 for MNIST and 0.01 for CIFAR-10 and Tiny-ImageNet. Unless otherwise specified, we add GBN in all layers.

Adversarial attacks. We follow existing guidelines [16, 17, 36] where we incorporate multiple adversarial attacks with different perturbation types and adopt their commonly-used settings for attacks. For MNIST, the magnitude of perturbation for ℓ_1 , ℓ_2 , and ℓ_∞ is $\epsilon = 10, 2, 0.3$. For CIFAR-10 and Tiny-ImageNet, the perturbation magnitude for ℓ_1 , ℓ_2 , and ℓ_∞ is $\epsilon = 12, 0.5, 0.03$. For ℓ_1 attacks, we adopt PGD [12], and BBA [60]; for ℓ_2 attacks, we use PGD, C&W [61], Gaussian noise [62], and boundary attack (BA) [63]; For ℓ_∞ attacks, we use PGD, FGSM [5], SPSA [25], Nattack [26], Momentum Iterative Method (MI-FGSM) [14], C&W, and AutoAttack [64]. To demonstrate that our GBN does not introduce obfuscated gradients, we use white-box and black-box adversarial examples, generated with both gradient-based and gradient-free algorithms.

Adversarial defenses. We compare with existing defenses against the union of ℓ_1 , ℓ_2 , ℓ_∞ adversaries. We compare with ABS [36]², MAX, AVG [16], and MSD [17]. For completeness, we also compare with TRADES [65], PAT [38], and PGD adversarial training [12] with a single perturbation type (*i.e.*, the model

²ABS considers the ℓ_0 perturbations, which are subsumed within the ℓ_1 ball of the same radius. Meanwhile, ABS is only designed for MNIST. Due to the limited code, we use the results reported in [36].

is trained on ℓ_1 , ℓ_2 , or ℓ_∞ , denoted as P_1 , P_2 , and P_∞ respectively).

Normalization techniques. We further compare our methods to existing normalization techniques, including MN and MBN. MN extends BN to more than a single mean and variance, detects the modes of the data, and then normalizes samples that share common features. MBN includes two BN branches for clean and adversarial examples respectively. Since manually selecting the BN branch is infeasible in the adversarial setting, we add a 2-way gated sub-network to each MBN block. We also evaluate the original MBN that only uses the clean BN during inference, which shows weak robustness (see Section 4.4).

Evaluation metrics. To evaluate model robustness against attacks, we report the **top-1 classification accuracy** for each adversarial attack method and clean examples (the higher the better). Since we use several adversarial attack methods, for each perturbation type (e.g., ℓ_1 , ℓ_2 , ℓ_∞), we measure the **worst-case top-1 classification accuracy** (the higher the better), where we report the worst result among various attacks within the perturbation type. In other words, given an input, if any attack within specific norm (e.g., ℓ_1) generates an adversarial example that leads to the wrong prediction, we mark it as a failure. Moreover, we also report **all attacks**, which represents the worst-case performance over all attacks of different perturbations for each input [17]. Similarly, given an image, if any attack generates an adversarial example that leads to the wrong prediction, we mark it as a failure.

GBN architectures. We here illustrate the architecture of the gated sub-network g in GBN. As shown in Figure 4, we devise two types of gated sub-network, namely *Conv gate* and *FC gate*. Here, the notation $\text{Conv2d}(d, s, k)$ refers to a convolutional layer with k filters whose size are $d \times d$ convolved with stride s ; $\text{ReLU}(\cdot)$ denotes the rectified linear unit used as the activation function in the network; and $\text{FC}(m)$ denotes a fully connected layer with output size m . Specifically, *Conv gate* is a convolutional neural network consisting of two convolutional layers, two ReLU layers, and one fully-connected layer; *FC gate* is a simple fully-connected neural network that includes two fully-connected layers and one ReLU layer.

Data availability statement. All our experiments are conducted on commonly adopted open datasets MNIST, CIFAR-10, and Tiny-ImageNet. For the implementation of defenses, we use the published

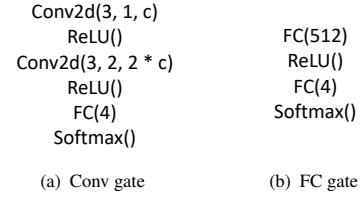


Fig. 4 The architecture of the gated sub-network.

codes for ABS³, MAX/AVG⁴, MSD⁵, TRADES⁶, and PAT⁷. For attacks, we use the original codes⁸ for AutoAttack, ART⁹ for C&W- ℓ_∞ , and ARES¹⁰ for SPSA and NATTACK; for other attacks we adopt FoolBox [62]. The code of our GBN can be found at <https://github.com/liuaishan/GBN>.

We defer more detailed implementation of GBN and hyper-parameters of our experiments to the supplementary material.

4.2 Comparison with other baselines

In this part, we first evaluate model robustness against multiple perturbation types (i.e., ℓ_1 , ℓ_2 , and ℓ_∞) in both the white-box and black-box settings. For all attacks except FGSM and APGD_{CE} (we use the default setting in AutoAttack), we ran 5 random restarts for each input. For GBN, we trained each model 3 times, and the results are similar.

The results on MNIST using LeNet, CIFAR-10 using ResNet-20, and Tiny-ImageNet using ResNet-34 are shown in Table 1. We also report the breakdown results for each individual attacks in the supplementary material. *Please refer to the supplementary materials for more experimental results on different datasets with different models.* Note that the results in Table 1 of each perturbation type indicate the sample-wise worst-case robustness, which would be slightly less than the worst robustness accuracy of these individual attacks in the breakdown results due to the computation strategy of the evaluation metrics. From these results, we can draw the following observations.

(1) For defending multiple perturbations (i.e., ℓ_1 , ℓ_2 , ℓ_∞) in both white-box and black-box scenarios, our GBN consistently outperforms others by large

³<https://github.com/bethgelab/AnalysisBySynthesis>

⁴<https://github.com/tramer/MultiRobustness>

⁵https://github.com/locuslab/robust_union

⁶<https://github.com/yaodongyu/TRADES>

⁷<https://github.com/cassidyaidlaw/perceptual-advex>

⁸<https://github.com/fra31/auto-attack>

⁹<https://github.com/Trusted-AI/adversarial-robustness-toolbox>

¹⁰<https://github.com/thu-ml/ares>

Table 1 Accuracies on different datasets (%). We emphasize both the best and second-best values for each type of attack for better visualization. We also provide the Standard Deviation for *All attacks* of each method.

(a) LeNet on MNIST

	Vanilla	PAT	TRADES	P_1	P_2	P_∞	AVG	MAX	ABS	MSD	MN	MBN	GBN(ours)
ℓ_1 attacks	5.1	50.3	9.6	32.6	67.3	7.1	30.2	26.6	/	41.2	23.1	60.5	72.8
ℓ_2 attacks	1.2	54.2	11.5	27.1	65.8	18.2	39.6	37.7	82.3	71.1	18.7	65.0	92.3
ℓ_∞ attacks	0.0	1.1	76.5	0.3	0.1	78.6	38.9	52.2	16.7	38.4	0.0	18.7	68.5
All attacks	0.0	1.0	9.2	0.1	0.1	6.9	29.4	26.3	16.3	38.1	0.0	18.4	68.5
	± 0.04	± 0.06	± 0.11	± 0.16	± 0.17	± 0.09	± 0.24	± 0.22	± 0.00	± 0.25	± 0.03	± 0.34	± 0.31
Clean	99.1	91.0	98.9	98.5	98.7	98.3	98.6	98.2	99.0	97.1	98.0	98.4	98.4

(b) ResNet-20 on CIFAR-10

	Vanilla	PAT	TRADES	P_1	P_2	P_∞	AVG	MAX	MSD	MN	MBN	GBN(ours)
ℓ_1 attacks	0.0	33.7	15.7	19.1	31.9	16.3	44.4	41.1	42.5	39.1	44.2	56.9
ℓ_2 attacks	0.0	47.7	59.1	54.7	55.8	50.1	55.7	51.6	58.2	29.5	20.0	68.5
ℓ_∞ attacks	0.0	24.8	44.6	11.7	23.5	37.6	30.2	33.7	37.6	12.7	39.7	49.2
All attacks	0.0	24.5	15.4	11.5	23.2	16.1	30.2	33.4	36.9	12.3	20.0	48.2
	± 0.03	± 0.36	± 0.35	± 0.05	± 0.41	± 0.36	± 0.50	± 0.42	± 0.56	± 0.51	± 0.61	± 0.64
Clean	89.4	62.2	86.2	83.7	87.2	83.6	80.0	76.7	78.4	82.0	79.1	80.2

(c) ResNet-34 on Tiny-ImageNet

	Vanilla	PAT	TRADES	P_1	P_2	P_∞	AVG	MAX	MSD	MN	MBN	GBN(ours)
ℓ_1 attacks	5.6	13.1	25.2	19.5	26.1	19.7	30.7	22.7	7.1	7.9	36.1	43.7
ℓ_2 attacks	10.1	12.7	31.2	29.6	32.5	27.9	32.2	27.5	11.0	17.4	30.4	41.6
ℓ_∞ attacks	0.0	2.2	9.3	0.3	0.5	9.0	6.5	8.1	5.0	6.4	19.3	38.2
All attacks	0.0	1.9	9.0	0.0	0.5	8.8	6.2	7.4	4.6	6.5	18.3	37.7
	± 0.05	± 0.35	± 0.44	± 0.21	± 0.37	± 0.52	± 0.56	± 0.58	± 0.67	± 0.62	± 0.52	± 0.63
Clean	54.0	20.2	43.0	52.3	54.1	44.1	41.2	35.9	28.5	46.3	45.5	43.2

margins over 10% absolute improvement on all 3 datasets. This demonstrates the superiority of our GBN approach to improving model robustness against multiple perturbations.

(2) Due to the trade-off between adversarial robustness and standard accuracy [66], our clean accuracy is lower than the vanilla model. However, our GBN maintains a comparatively high clean accuracy compared to other adversarial defense strategies.

(3) GBN is easy to train on different datasets, while other defenses for multiple perturbation types (e.g., MSD) are hard to converge on large datasets such as Tiny-ImageNet. This further indicates the training advantage of our GBN.

(4) Based on the results of black-box and gradient-free adversarial attacks in our supplementary material (i.e., BA, SPSA, NATTACK), GBN outperforms the others by large margins, confirming that no gradient masking [67] has been introduced.

(5) In contrast to other normalization methods, as shown in Table 1, GBN outperforms MN and MBN by

large margins (up to 60% absolute improvement). We conjecture that the key factor behind is that MN and MBN do not align the feature representations for different data distributions (different ℓ_p -norm perturbations). Specifically, MN aims to preserve the diversity among different distributions, by learning the mixture of Gaussian; as for the modified MBN, the data from different perturbation types are mixed in the same BN. For our GBN, it first aligns the distribution among different perturbations by using one BN branch to handle one perturbation type (learn domain-specific features), and then the aligned distribution contributes to the subsequent modules or layers (e.g., convolutional layer) for learning domain-invariant representations. More discussions can be found in Section 5.2.

4.3 Adaptive white-box attacks for GBN

Besides the commonly-adopted adversarial attacks, we here examine the performance of GBN against white-box attacks specially designed for GBN, aiming to provide a more rigorous analysis. In the following

cases, the adversary knows every detail of our GBN and could directly attack the GBN block.

In particular, we conduct the following experiments: (1) attacking the gated sub-networks, *i.e.*, generating adversarial examples to fool the classification of the gated sub-networks; (2) manually selecting the BN branch to generate adversarial examples; (3) generate adversarial attacks by optimizing jointly the model final prediction and the gated sub-network; and (4) generate adversarial attacks by randomly attacking with ℓ_1 , ℓ_2 , and ℓ_∞ -norm perturbations.

First type of adaptive attack. Given clean, ℓ_1 , ℓ_2 , and ℓ_∞ adversarial examples, we then perturb these samples to fool the gated sub-networks at all layers of ResNet-20 on CIFAR-10 using PGD attacks. Our whole model achieves 73.2%, 71.4%, 72.4%, and 71.8% classification accuracy for fooling the gated sub-networks to wrong predictions towards clean, ℓ_1 , ℓ_2 , and ℓ_∞ domains.

Second type of adaptive attack. Here, the adversary generates adversarial examples by manually selecting the BN branch of the GBN module to perform PGD attacks. In Table 2, GBN remains the same level of robustness on both MNIST and CIFAR-10 dataset compared to our main white-box attacks.

Third type of adaptive attack. Here, we choose ResNet-20 and the CIFAR-10 dataset, where we generate adversarial attacks by optimizing jointly the model final prediction and the gated sub-network. In other words, we attack the final outputs of the model to generate ℓ_1 , ℓ_2 , and ℓ_∞ adversarial examples; meanwhile we also force the outputs of all sub-networks to wrong branch predictions, which is inconsistent with the branch of the adversarial examples. As shown in Table 3, the third type of adaptive attack achieves the strongest attacking ability among the three attacks and could attack our GBN to some extent. However, the robust accuracy of GBN under this type of attack does not decrease too much.

Fourth type of adaptive attack. Given clean examples, we set the overall PGD attack step number as 100. At each iteration step, we generate attacks by randomly choosing ℓ_1 , ℓ_2 , and ℓ_∞ bounded perturbations and perform clip operation based on the average constraint among the three types. The ResNet-20 model with GBN on CIFAR-10 achieves 57.1% accuracy in this scenario.

Discussions. Based on the above results, we can draw several conclusions as follows.

Table 2 Second type of adaptive attack. White-box attacks on MNIST with LeNet and CIFAR-10 with ResNet-20 by manually selecting BN branches to generate adversarial examples (BN⁰, BN¹, BN², and BN³ denotes the BN branch for clean, ℓ_1 , ℓ_2 , and ℓ_∞ adversarial examples in GBN). Results are shown in model accuracy (%).

	MNIST				CIFAR-10			
	BN ⁰	BN ¹	BN ²	BN ³	BN ⁰	BN ¹	BN ²	BN ³
PGD- ℓ_1	86.7	86.3	86.5	96.7	58.2	58.0	58.7	59.7
PGD- ℓ_2	97.6	98.0	97.2	97.8	69.2	69.3	68.8	69.2
PGD- ℓ_∞	96.8	97.8	96.2	95.8	60.1	60.7	60.7	59.5
Clean accuracy	98.4	98.4	98.4	98.4	80.2	80.2	80.2	80.2

Table 3 Third type of adaptive attack. (a) shows the classification accuracy (%) of ResNet-20 on CIFAR-10 against attacks that jointly fool model prediction and gated sub-network. (b) shows the results of standard white-box PGD attacks.

(a) Third type of adaptive attack using LeNet on MNIST				
	Clean	Adaptive PGD- ℓ_1	Adaptive PGD- ℓ_2	Adaptive PGD- ℓ_∞
GBN	80.2	56.5	50.6	55.4

(b) Standard white-box attack on MNIST and CIFAR-10						
	MNIST			CIFAR-10		
	PGD- ℓ_1	PGD- ℓ_2	PGD- ℓ_∞	PGD- ℓ_1	PGD- ℓ_2	PGD- ℓ_∞
GBN	86.1	97.4	95.8	58.1	68.9	58.0

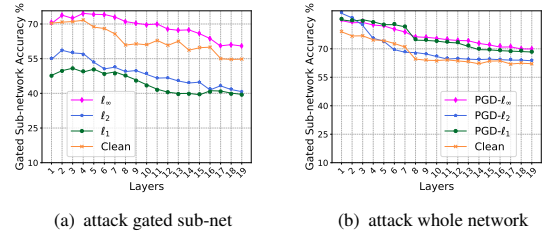


Fig. 5 Gated sub-network prediction accuracy in different scenarios (ResNet-20 on CIFAR-10). The x-axis denotes the serial number of layers in the ResNet-20 model, and each point in the figure represents the prediction value of the gated sub-network at specific layer of ResNet-20. (a) shows the results of fooling gated sub-networks in all GBN layers (the first type of adaptive attack); (b) shows the results of attacking whole network (common white-box attacks for the model).

(1) Our GBN does not rely on obfuscated gradient to provide robustness to models [67]. Obfuscated gradient or gradient masking has been demonstrated to cause a false sense of security, which often shows high accuracy on standard white-box attacks while low performance on adaptive attacks. The robustness of GBN decreases on adaptive attacks but still remains comparatively stable, which specifies that our GBN does not introduce obfuscated gradient.

(2) Compared to attacking the full model, as done in Table 1, the model accuracy towards the first and second adaptive attacks are at the same level or comparatively higher. We conjecture that the reasons might be listed as follows. For the *first adaptive attack*, different GBN layers use different features to predict the domains, thus it is difficult to simultaneously fool all GBN layers under the magnitude constraint (see Figure 5(a) for gated sub-networks prediction accuracy using the first type of attack). For example, the prediction accuracies of the gated sub-networks at different layers (each point in Figure 5(a)) are almost all higher than 40% after being attacked. Even if being able to fool all the gated sub-networks and force the adversarial examples to wrong BN branches during inference, the attack is similar to generating and feeding white-box adversarial examples for adversarially-trained models with single BN (such as AVG), since the adversarial examples are all normalized by the “wrong” BN branch for AVG. According to the results in the supplementary materials, the results of the first adaptive attack on GBN and common white-box PGD attacks on AVG are also similar. As for the *second type of adaptive attack*, we conjecture that the BN branches during adversarial examples generation might not be critical for the adversarial attacking ability. The common white-box attacks (our main experiments) generate adversarial examples based on gradients via test mode BN, which would go through the corresponding BN branches that are most likely to maximize the model loss. Thus, the second adaptive attack shows relatively lower attacking performance than common white-box attacks.

(3) The third type of attack achieves the best-attacking performance and outperforms most of the common white-box attacks. Though showing weaker performance than the third one, the fourth type of adaptive attack achieves comparatively high attacking performance. Similarly, the fourth type of adaptive attack aims to mislead the overall model output, meanwhile, it also achieves the effect to fool the gated sub-network since the combination of perturbation types might be hard for GBN to classify. Therefore, it suggests that the weak point of our GBN might be attacked and exploited by adversaries that simultaneously fool the GBN prediction and model prediction.

4.4 Ablation study

In this section, we provide some ablation studies to further investigate our GBN approach.

Table 4 Model accuracy (%) of ResNet-20 on CIFAR-10 on different PGD- k attacks (k is the iteration steps).

	Vanilla	TRADES	AVG	MAX	MSD	MN	MBN	GBN(ours)
PGD-50	2.3	49.5	37.1	40.4	44.1	34.1	58.4	59.5
PGD-100	0.0	49.4	36.5	39.8	43.5	33.8	57.7	59.2
PGD-200	0.0	48.8	36.1	38.9	43.0	33.2	57.1	58.6
PGD-1000	0.0	47.5	35.2	38.6	42.2	32.1	54.8	58.0

Table 5 Accuracy (%) of GBN under white-box PGD- ℓ_1 , PGD- ℓ_2 , and PGD- ℓ_∞ attacks with different perturbation budgets.

(a) PGD- ℓ_1							
ϵ	3	6	12	24	36	48	60
PGD- ℓ_1	74.7	66.1	58.1	46.5	37.5	25.5	16.5
(b) PGD- ℓ_2							
ϵ	0.125	0.25	0.5	1	2	3	4
PGD- ℓ_2	76.4	72.1	68.9	58.5	48.2	36.4	24.3
(c) PGD- ℓ_∞							
ϵ	2/255	4/255	8/255	16/255	24/255	32/255	40/255
PGD- ℓ_∞	70.5	62.2	58.0	47.9	35.8	22.4	15.7

Different attack steps and budgets. In this part, we evaluate and show the behavior of our GBN towards adversarial attacks with different iteration steps and perturbation budgets.

Firstly, we provide the experimental results of PGD adversarial attacks using different iteration step numbers (*i.e.*, 50, 100, 200, 1000) in terms of ℓ_∞ norm on CIFAR-10. For PGD attacks, we set the perturbation budgets $\epsilon=0.03$, step size $\alpha=\epsilon/10$, and different iteration steps k . In general, with the increasing of the iteration steps, the attacks become stronger. As shown in Table 4, our GBN still outperforms other methods on PGD attacks using different iteration steps and remains a high level of robustness.

Moreover, we conduct experiments using PGD attacks of different perturbation budgets on CIFAR-10. Specifically, we choose ResNet-20 and use white-box PGD- ℓ_1 , PGD- ℓ_2 , and PGD- ℓ_∞ attacks with 7 different perturbation budgets. The specific budgets and results are shown in Table 5. From the results we can observe that the robustness of GBN decreases with the increasing of perturbation budgets but it could still keep robustness to a certain extent.

Effectiveness of the gated sub-network. As a core part of our GBN block, the performance of the

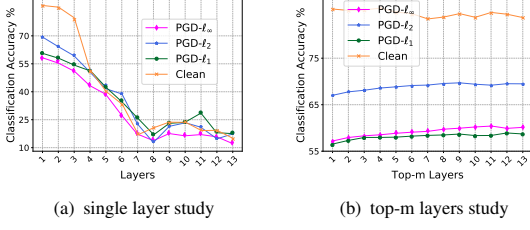


Fig. 6 Adding GBN to different layers (VGG-16 on CIFAR-10): (a) shows the results of adding GBN to single layers; (b) shows the results of adding GBN to top- m layers.

gated sub-network plays a critical role in adversarial defense. Therefore, in this part, we provide a deeper understanding of GBN by investigating the gated sub-networks performance. Specifically, we conduct two experiments as (1) we report classification accuracies of the gated sub-network of our GBN for different perturbation types (domains), and (2) we remove the 2-way gated sub-network of MBN (denoted as “vanilla MBN”) and follow the original implementation [51] by only using the clean BNs for inference. For the *first experiment*, against common white-box attacks (Figure 5(b)), the prediction accuracy of the gated sub-network drops with the increasing of the layer depth. The reason might be that low-level statistics learned in shallow layers are easier to train [68], while the features from different domains are more and more entangled as the layer depth increases, making it harder for models to separate them. For the *second experiment*, the accuracies of vanilla MBN on CIFAR-10 with ResNet-20 against white-box PGD- ℓ_1 , PGD- ℓ_2 , and PGD- ℓ_∞ attacks are 21.3%, 44.8%, 33.7%, which show significantly worse robustness compared to MBN with gated sub-network and our GBN (see Table 1(b)). To sum up, the above experiments demonstrate the efficacy of the gated sub-network and we suggest improving the gated sub-network prediction accuracy to further improve model robustness.

Adding GBN to different layers. Here, we try to add GBN blocks at different layers of the model. Firstly, we add GBN to different single layers. In other words, we only add GBN to a single layer and then adversarially train the model. As shown in Figure 6(a), the standard performance and adversarial robustness decrease as we only add GBN into the deeper layers. The reasons might be: (1) shallow layers are more critical to model robustness [35] and (2) the features from different domains (*i.e.*, different ℓ_p -norm adversarial examples and clean examples) are highly entangled in the deeper layers, which might be

harder to separate (*see Supplementary Materials for the running statistics at deeper layers of the model*).

We then add GBN to layer groups (*i.e.*, top- m layers). As shown in Figure 6(b), the model robustness improves as more layers are involved, while the clean accuracy remains comparatively stable. Therefore, we add GBN in all layers by default.

Using gated sub-network only in the first GBN.

After investigating the performance of GBN on different model layers, we conduct extra experiments by only using a gated sub-network in the first GBN block. In other words, we only include gated sub-network in the first GBN layer, and then send the soft-labels to the following layers. Specifically, the following GBN layers do not contain gated sub-networks and only depend on the prediction results of the first GBN layer to classify the input domains.

The accuracy of a ResNet-20 on CIFAR-10 against PGD- ℓ_1 , PGD- ℓ_2 , PGD- ℓ_∞ adversarial examples, and clean examples are 57.3%, 67.1%, 57.7%, and 83.5%, which is slightly weaker than our implementation. Thus, we use our original implementations in our main experiments (adding gated sub-networks in each GBN layer). We conjecture the reasons as (1) Model parameter sizes. The model parameter sizes for models with gated sub-networks in the first blocks and in all blocks are 0.3M and 8.8M, respectively. Since larger parameter sizes within the same model family often indicate better robustness [69], models added GBNs in all layers contain larger parameter sizes and in turn show better robustness. However, we should also notice that these additional parameters contribute primarily to the domain prediction of gated sub-network than the final model classification. (2) Prediction differs at different layers. Given an input, the weights for each domain of the gated sub-network in each layer are not the same for the best defense performance. For more studies, we put them as future work.

Replacing BN branches with MLP branches in GBN. In addition, we try to investigate the critical role of BN branches in our GBN, where we conduct ablations using ResNet-20 on the CIFAR-10 dataset by replacing the BN branches with MLP branches. In particular, we replace the BN branches after the gated subnetwork with a convolution layer (we set the kernel size as 3*3, stride as 1, and the input channel the same as the output channel). However, since there are no BN layers, the training is unstable and could not converge, which further demonstrate the importance of BN in our GBN approach.

5 Discussion and Analysis

5.1 Multi-domain hypothesis

Here, we provide deeper understanding and verification of our multi-domain hypothesis.

Visualization of running statistics on different models. In this part, we provide more running statistics of different deep models to further verify our multi-domain hypothesis. In particular, we train a VGG-16, WideResNet-28-10, ResNet-20, and WideResNet-34-10 model with the multiple BN branch structure. The running statistics of each BN branch at different layers (16 randomly selected channels) are shown in Figure 7. From the results, we can further observe that different perturbation types induce different BN statistics, which may arise in different domains.

Fourier perspective analysis To verify our multi-domain hypothesis, we study the differences between perturbation types from the Fourier perspective [70]. We visualize the Fourier heatmap following [70] on 4 different ResNet-20 models (*i.e.*, a vanilla model and 3 adversarially-trained models using only ℓ_1 , ℓ_2 , and ℓ_∞ adversarial examples, respectively) and shift the low frequency components to the center of the spectrum. Error rates are averaged over 1000 randomly sampled images from the test set on CIFAR-10. The redder the zone, the higher the error rate of the model to perturbations of specific frequency.

As shown in Figure 8, models trained using different ℓ_p perturbations demonstrate different model weaknesses in the Fourier heatmap (*i.e.*, different hot zones). For example, model trained on PGD- ℓ_2 is more susceptible to high-frequency perturbations while less susceptible to some low-frequency perturbations (the smaller blue zone in the center), while model trained on PGD- ℓ_∞ is comparatively more robust to middle-frequency perturbations (light yellow zones). Therefore, different perturbation types have different frequency properties, and models trained on different perturbations are sensitive to perturbations from different frequencies. This observation further demonstrates that different perturbation types may arise from different domains.

Training with different ratios of perturbation types on a single BN. Our Theorem 1 demonstrates that training with a mixture of perturbation types on a single BN would cause an inevitable domain gap between training and testing data, which causes the performance degeneration. To verify this, we hereby

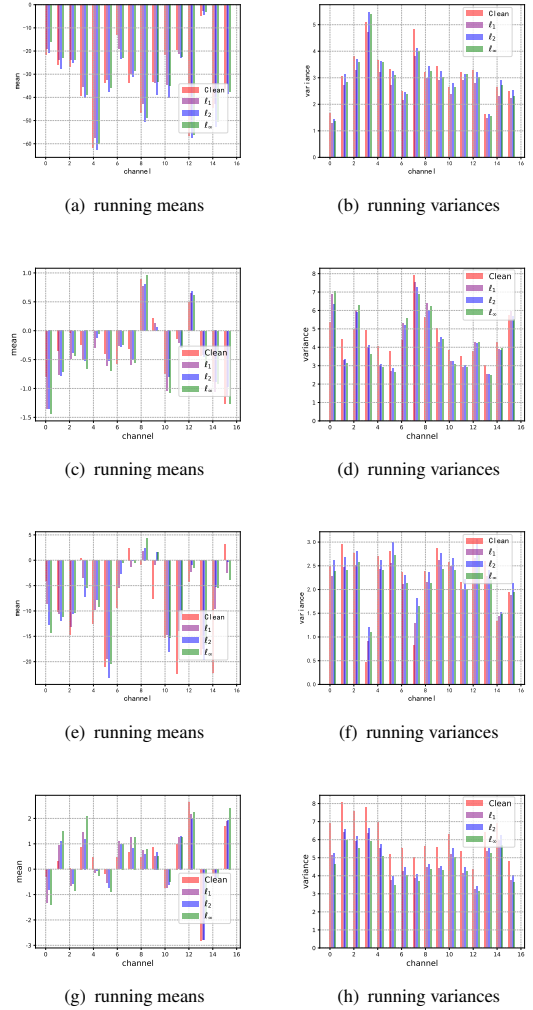


Fig. 7 Running statistics (running mean and variance) of each BN in the multiple BN branches at different layers on models trained on CIFAR-10. Here, we randomly choose 16 channels for visualization. (a) and (b) show the layer *conv3_1* on VGG-16; (c) and (d) denote the layer *block1.layer1.bn2* on WideResNet-28-10; (e) and (f) denote the layer *layer1.1.bn1* on ResNet-20; (g) and (h) denote the layer *block1.layer1.bn2* on WideResNet-34-10.

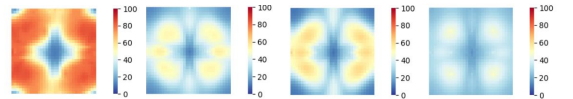


Fig. 8 Fourier analysis on model sensitivity to additive noise aligned with different Fourier basis vectors on CIFAR-10. From left to right: vanilla model, PGD- ℓ_1 trained model, PGD- ℓ_2 trained model, and PGD- ℓ_∞ trained model. The numbers indicate the model error rates.

train several individual models with different ratios of perturbation types for the estimation of the single BN layer while using the same perturbation type (*i.e.*, ℓ_1) to update the convolution layers of the model. Specifically, for each individual model with a single BN, we use different ratios of perturbation types (*e.g.*, clean, ℓ_1 , ℓ_2 , and ℓ_∞ adversarial examples) to estimate the running statistics of BN, but only use ℓ_1 adversarial examples to optimize the model parameters (*e.g.*, convolutions). For model M_1 , we use ℓ_1 adversarial examples to estimate the running statistics of the BN layer; for model M_2 , we use ℓ_1 and ℓ_2 adversarial examples to estimate the running statistics of the BN layer; for model M_3 , we use clean example, ℓ_1 , and ℓ_∞ adversarial examples to estimate the running statistics of the BN layer; for model M_4 , we use clean example, ℓ_1 , and ℓ_∞ adversarial examples to estimate the running statistics of the BN layer; for model M_5 , we use clean example, ℓ_1 , ℓ_2 , and ℓ_∞ adversarial examples to estimate the running statistics of the BN layer. For all these models, we use ℓ_1 adversarial examples to optimize the model weights, and we keep the same amount of training data. For all these models, they use different ratios of perturbations to estimate the BN layer, and use the same data to optimize the model weight. Thus, we could control the variables and the differences between these models (M_1 to M_5) are the estimation of BN layer.

On CIFAR-10, the predication accuracy for PGD- ℓ_1 attacks (the same settings for our main experiment) from M_1 to M_5 is shown as: **92.5%**, 84.0%, 89.1%, 85.5%, and 83.8%, respectively. M_1 achieves the strongest robustness on ℓ_1 attacks, which empirically verify our Theorem 1 that the model achieves the best performance when the proportion of the different perturbations in the training set is most close to that in the test set. Thus, we should not learn a mixture distributions with a single BN.

5.2 Feature visualization before/after normalization

In this part, we aim to better understand the effect of our GBN via feature visualization. Specifically, we use t-SNE [71] to visualize the features before and after the normalization. As shown in Figure 9, the features of different domains are aligned to domain-invariant representations after GBN, *i.e.*, one clean example (the red dot) and its corresponding adversarial examples (the blue, green, and yellow dots) tend to be close in the space of normalized output. However, after the

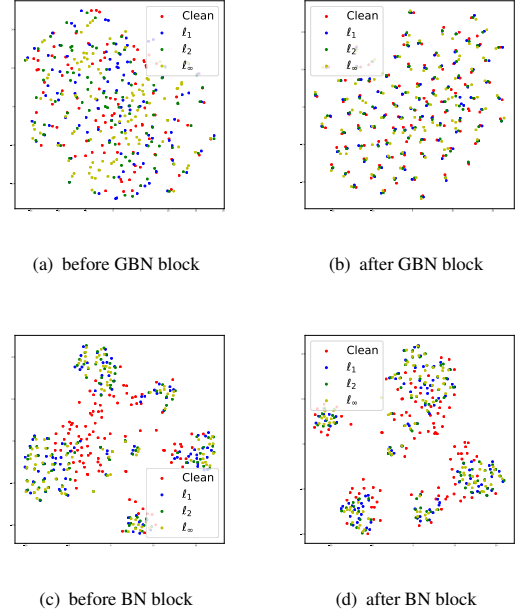


Fig. 9 Feature visualization. We use the BN block at layer *conv3_1* of a VGG-16 model trained using AVG (c-d), and the GBN block at layer *conv3_1* of a VGG-16 (a-b). We visualize the features before and after BN/GBN blocks. Features of different domains are aligned to domain-invariant representations after GBN, while distances between the clean example and its corresponding adversarial examples are still far after BN.

BN block of AVG, distances between the clean example and its corresponding adversarial examples are still far. All the above experiments are conducted on CIFAR-10 with VGG-16.

Therefore, we can draw an important conclusion that our GBN provides model robustness against multiple perturbation types by normalizing them into aligned features for better learning. In particular, GBN first aligns the distribution among different perturbations types by using one BN branch to handle one perturbation type (learn domain-specific features), and then the aligned distribution contributes to the subsequent modules or layers (*e.g.*, convolutional layer) for learning domain-invariant representations.

5.3 Defending unseen ℓ_p perturbations

Finally, we examine the generalization of GBN to unseen ℓ_p bounded adversarial perturbations. In other words, during testing, the model may encounter the types of adversarial examples that has never been trained on. Specifically, we train a variant of GBN that only includes 3 BN branches. These GBN models are trained on two ℓ_p perturbations only, but are evaluated

Table 6 Classification accuracy (%) of ResNet-20 on CIFAR-10, where models need to generalize to attack types not included for training (the higher the better). “ $\ell_1+\ell_2+\ell_\infty$ ”, “ $\ell_1+\ell_\infty$ ”, and “ $\ell_2+\ell_\infty$ ” denote models trained on different combinations of perturbation types.

	Clean	PGD- ℓ_1	PGD- ℓ_2	PGD- ℓ_∞
Vanilla	0.1	0.0	0.0	89.4
$\ell_1+\ell_2+\ell_\infty$	AVG	80.0	47.8	57.2
	MAX	76.7	43.9	54.3
	MSD	78.4	49.3	62.3
	MN	82.0	43.7	48.9
	MBN	79.1	47.3	60.1
	GBN	80.2	58.1	68.9
$\ell_1+\ell_\infty$	AVG	74.2	50.2	58.7
	MSD	71.2	49.4	60.0
	MN	83.1	41.0	47.2
	MBN	80.3	47.8	58.4
	GBN	81.1	57.1	64.1
$\ell_2+\ell_\infty$	AVG	77.0	30.0	57.7
	MSD	73.0	23.2	56.1
	MN	82.0	25.1	47.4
	MBN	79.4	30.1	58.9
	GBN	80.8	40.3	64.7

Table 7 GBN in batch-unrelated normalization scenario. Results are shown using accuracy (%) of ResNet-20 on CIFAR-10 on different types of perturbations.

(a) Comparison with models trained on single GN, LN, and IN				
	Clean	PGD- ℓ_1	PGD- ℓ_2	PGD- ℓ_∞
GBN(ours)	80.2	58.1	68.9	58.0
BN	80.0	47.8	57.2	35.2
GN	76.4	48.7	57.5	35.2
LN	75.9	47.6	58.1	36.0
IN	67.9	46.4	53.9	32.8

(b) Replacing LN with GBN				
	Clean	PGD- ℓ_1	PGD- ℓ_2	PGD- ℓ_∞
ViT_{GBN}	81.0	44.5	51.9	49.9
ViT _{LN}	78.8	38.9	31.2	46.1

on all the three ℓ_p perturbations, including the unseen perturbation.

As shown in Table 6, unsurprisingly, compared to the full GBN model with 4 BN branches and trained on (clean examples, ℓ_1 , ℓ_2 , and ℓ_∞ adversarial examples), the robustness of the held-out perturbation type decreases. However, the robustness is still significantly better than other baselines with the same setting, and sometimes even outperforms others that are trained on all perturbation types.

5.4 Batch-unrelated normalization scenario

In contrast to BN that computes statistics on the batch of samples, there also exists several normalization techniques that use batch-unrelated information for estimating normalization statistics such as Group Normalization (GN) [72], Instance Normalization (IN) [73], and Layer Normalization (LN) [74]. Therefore, we further investigate the potential and effectiveness of our GBN in the batch-unrelated scenario.

Adversarial training for GN/IN/LN. We first adversarially train models with the batch-unrelated normalization layer GN, LN, and IN, so that we could avoid exploiting the batch dimension to calculate statistics. Specifically, we replace all the GBN blocks in ResNet-20 with GN or IN and adversarially train the models on CIFAR-10 using AVG. For GN, we split the channel into 4 groups; for LN and IN, we use the default setting. From the results in Table 7(a) we can observe that the robust accuracy for ResNet-20 with GN/LN/IN under PGD- ℓ_1 , PGD- ℓ_2 , and PGD- ℓ_∞ attacks are much lower than ResNet-20 with GBN blocks, which demonstrates the effectiveness of our GBN. Meanwhile, we also found that (1) single GN achieves slightly better robustness than single BN, which somewhat reveals the fact that erasing the adversarial domain-related statistics may help improve the robustness for adversarial training; and (2) single IN shows the lowest performance on both clean and adversarial examples, which might be caused by its strict sample-wise constraints that influence the model learning ability.

Replacing LN with GBN. In addition, we try to study whether the concept of GBN can be transferred to other normalization layers. Specifically, we select the Vision Transformers (ViTs) architecture [75] that uses LN as default and replace the LN layers with our GBN layers; we then adversarially train the ViT with GBN (denoted as “ViT_{GBN}”). We also report the results of adversarial training on ViT with LN (denoted as “ViT_{LN}”) using AVG. As shown in Table 7(b), on CIFAR-10, the robust accuracies for ViT with GBN blocks are higher than ViT with LNs, which further demonstrates the potential of our GBN in other normalization layers. We will explore the possibilities of extending our motivation to GLN (gated layer normalization) in the future.

Table 8 Training and inference time evaluation of different methods using ResNet-20 on CIFAR-10.

	AVG	MAX	MSD	MN	MBN	GBN(ours)
Training speed (seconds/ epoch)	1837.9	1113.2	689.8	19329.1	2737.9	2802.6
Training duration (hours)	20.4	12.4	7.7	214.8	30.4	31.1
Inference speed (seconds/ 10000 images)	0.6	0.6	0.6	4.8	1.9	2.0

5.5 Computational overhead

Since our method imports additional blocks into DNNs, we further analyze its computational cost in this part. As for the parameters, in each layer, we have $N+1$ pairs of $\{\hat{\mu}, \hat{\sigma}\}$ to estimate compared to one pair of standard BN (other baselines also adopt models that contain standard BN layers); our GBN also introduces extra learnable parameters θ in the gated sub-network.

We then empirically evaluate the time consumption during training and inference for our GBN and other defenses. All the experiments are conducted on an NVIDIA Tesla V100 GPU cluster. We compute the overall training time using ResNet-20 on CIFAR-10 for 40 epochs and the inference time for 10000 images. According to the results in Table 8, our GBN spends the comparative time during training and inference with other adversarial defenses. During training, our GBN has extra parameters θ in the gated sub-network to learn. However, the most time-consuming procedure of adversarial training involves generating adversarial examples. Therefore, our training time cost is comparable to other adversarial defense baselines. As for the inference, our GBN requires to classify the input samples into the specific domain using the gated sub-network. Therefore, our method is slightly slower than methods that are solely training the models (e.g., AVG). However, we achieve similar and even faster speeds compared to other methods that require run-time predictions on input domains (e.g., MN). Therefore, though extra parameters are introduced, our GBN achieves comparable time cost to other defenses.

6 Conclusions

Most adversarial defenses are tailored to a single perturbation type (e.g., small ℓ_∞ -noise), but offer no guarantees against multiple ℓ_p bounded adversarial attacks. To better understand this phenomenon,

we explored the *multi-domain* hypothesis that different ℓ_p bounded adversarial perturbations are drawn from different domains. Thus, we propose a novel building block for DNNs, *Gated Batch Normalization* (GBN), which consists of a gated network and a multi-branches BN layer. The gated sub-network separates different perturbation types, and each BN branch is in charge of a single perturbation type and learns the domain-specific statistics for input transformation. Then, features from different branches are aligned as domain-invariant representations for the subsequent layers. Extensive experiments on MNIST, CIFAR-10, and Tiny-ImageNet demonstrate that our GBN outperforms previous proposals against ℓ_1 , ℓ_2 , and ℓ_∞ adversarial attacks by large margins.

Though promising, our GBN block introduces extra parameters and requires additional computation, and we will investigate ways to accelerate training in future work. Also, we are interested in applying GBN in more complex scenarios to defend other unseen noises (e.g., common corruptions).

7 Acknowledge

This work was supported by National Natural Science Foundation of China (62206009, 62022009, and 61872021), and the National Key Research and Development Plan of China (2020AAA0103502).

References

- [1] Alex Krizhevsky, Ilya Sutskever, and Geoffrey E. Hinton. Imagenet classification with deep convolutional neural networks. In *International Conference on Neural Information Processing Systems*, 2012.
- [2] Dzmitry Bahdanau, Kyunghyun Cho, and Yoshua Bengio. Neural machine translation by jointly learning to align and translate. *arXiv preprint arXiv:1409.0473*, 2014.
- [3] Geoffrey Hinton, Li Deng, Dong Yu, George E. Dahl, Abdelrahman Mohamed, Navdeep Jaitly, Andrew Senior, Vincent Vanhoucke, Patrick Nguyen, and Tara N. Sainath. Deep neural networks for acoustic modeling in speech recognition: The shared views of four research groups. *IEEE Signal Processing Magazine*, 2012.

- [4] Christian Szegedy, Wojciech Zaremba, Ilya Sutskever, Joan Bruna, Dumitru Erhan, Ian Goodfellow, and Rob Fergus. Intriguing properties of neural networks. *arXiv preprint arXiv:1312.6199*, 2013.
- [5] Ian J Goodfellow, Jonathon Shlens, and Christian Szegedy. Explaining and harnessing adversarial examples (2014). *arXiv preprint arXiv:1412.6572*, 2014.
- [6] Alexey Kurakin, Ian Goodfellow, and Samy Bengio. Adversarial examples in the physical world. *arXiv preprint arXiv:1607.02533*, 2016.
- [7] Aishan Liu, Xianglong Liu, Jiaxin Fan, Yuqing Ma, Anlan Zhang, Huiyuan Xie, and Dacheng Tao. Perceptual-sensitive gan for generating adversarial patches. In *33rd AAAI Conference on Artificial Intelligence*, 2019.
- [8] Aishan Liu, Tairan Huang, Xianglong Liu, Yitao Xu, Yuqing Ma, Xinyun Chen, Stephen Maybank, and Dacheng Tao. Spatiotemporal attacks for embodied agents. In *European Conference on Computer Vision*, 2020.
- [9] Nicolas Papernot, Patrick Mcdaniel, Xi Wu, Somesh Jha, and Ananthram Swami. Distillation as a defense to adversarial perturbations against deep neural networks. *arXiv preprint arXiv:1511.04508*, 2015.
- [10] Logan Engstrom, Andrew Ilyas, and Anish Athalye. Evaluating and understanding the robustness of adversarial logit pairing. *arXiv preprint arXiv:1807.10272*, 2018.
- [11] Chongzhi Zhang, Aishan Liu, Xianglong Liu, Yitao Xu, Hang Yu, Yuqing Ma, and Tianlin Li. Interpreting and improving adversarial robustness with neuron sensitivity. *IEEE Transactions on Image Processing*, 2020.
- [12] Aleksander Madry, Aleksandar Makelov, Ludwig Schmidt, Dimitris Tsipras, and Adrian Vladu. Towards deep learning models resistant to adversarial attacks. In *International Conference on Learning Representations*, 2018.
- [13] Alexey Kurakin, Ian Goodfellow, and Samy Bengio. Adversarial machine learning at scale. In *International Conference on Learning Representations*, 2017.
- [14] Yinpeng Dong, Fangzhou Liao, Tianyu Pang, and Hang Su. Boosting adversarial attacks with momentum. In *IEEE Conference on Computer Vision and Pattern Recognition*, 2018.
- [15] Daniel Kang, Yi Sun, Dan Hendrycks, Tom Brown, and Jacob Steinhardt. Testing robustness against unforeseen adversaries. *arXiv preprint arXiv:1908.08016*, 2019.
- [16] Florian Tramèr and Dan Boneh. Adversarial training and robustness for multiple perturbations. In *Advances in Neural Information Processing Systems*, 2019.
- [17] Pratyush Maini, Eric Wong, and Zico J. Kolter. adversarial robustness against the union of multiple perturbation model. In *International Conference on Machine Learning*, 2020.
- [18] Aishan Liu, Jiakai Wang, Xianglong Liu, Bowen Cao, Chongzhi Zhang, and Hang Yu. Bias-based universal adversarial patch attack for automatic check-out. In *ECCV*, 2020.
- [19] Francesco Croce, Jonas Rauber, and Matthias Hein. Scaling up the randomized gradient-free adversarial attack reveals overestimation of robustness using established attacks. *International Journal of Computer Vision*, 2020.
- [20] Xingxing Wei, Huanqian Yan, and Bo Li. Sparse black-box video attack with reinforcement learning. *International Journal of Computer Vision*, 2022.
- [21] Tom B Brown, Dandelion Mané, Aurko Roy, Martín Abadi, and Justin Gilmer. Adversarial patch. *arXiv preprint arXiv:1712.09665*, 2017.
- [22] Jiakai Wang, Aishan Liu, Zixin Yin, Shunchang Liu, Shiyu Tang, and Xianglong Liu. Dual attention suppression attack: Generate adversarial camouflage in physical world. In *CVPR*, 2021.
- [23] Ranjie Duan, Xiaofeng Mao, A Kai Qin, Yuefeng Chen, Shaokai Ye, Yuan He, and Yun Yang. Adversarial laser beam: Effective physical-world

- attack to dnns in a blink. In *CVPR*, 2021.
- [24] Siyuan Liang, Xingxing Wei, Siyuan Yao, and Xiaochun Cao. Efficient adversarial attacks for visual object tracking. In *Computer Vision—ECCV 2020: 16th European Conference, Glasgow, UK, August 23–28, 2020, Proceedings, Part XXVI 16*, pages 34–50. Springer, 2020.
- [25] Jonathan Uesato, Brendan O’Donoghue, Aäron van den Oord, and Pushmeet Kohli. Adversarial risk and the dangers of evaluating against weak attacks. In *International Conference on Machine Learning*, 2018.
- [26] Yandong Li, Lijun Li, Liqiang Wang, Tong Zhang, and Boqing Gong. Nattack: Learning the distributions of adversarial examples for an improved black-box attack on deep neural networks. In *International Conference on Machine Learning*, 2019.
- [27] Aishan Liu, Jun Guo, Jiakai Wang, Siyuan Liang, Renshuai Tao, Wenbo Zhou, Cong Liu, Xianglong Liu, and Dacheng Tao. X-adv: Physical adversarial object attacks against x-ray prohibited item detection. In *USENIX Security Symposium*, 2023.
- [28] Xingxing Wei, Siyuan Liang, Ning Chen, and Xiaochun Cao. Transferable adversarial attacks for image and video object detection. *arXiv preprint arXiv:1811.12641*, 2018.
- [29] Siyuan Liang, Baoyuan Wu, Yanbo Fan, Xingxing Wei, and Xiaochun Cao. Parallel rect-angle flip attack: A query-based black-box attack against object detection. *arXiv preprint arXiv:2201.08970*, 2022.
- [30] Cihang Xie, Jianyu Wang, Zhishuai Zhang, Zhou Ren, and Alan Yuille. Mitigating adversarial effects through randomization. In *International Conference on Learning Representations*, 2018.
- [31] Fangzhou Liao, Ming Liang, Yinpeng Dong, Tianyu Pang, Xiaolin Hu, and Jun Zhu. Defense against adversarial attacks using high-level representation guided denoiser. In *IEEE Conference on Computer Vision and Pattern Recognition*, 2018.
- [32] Moustapha Cisse, Piotr Bojanowski, Edouard Grave, Yann Dauphin, and Nicolas Usunier. Parsenal networks: Improving robustness to adversarial examples. In *International Conference on Machine Learning*, 2017.
- [33] Gaurav Goswami, Akshay Agarwal, Nalini Ratha, Richa Singh, and Mayank Vatsa. Detecting and mitigating adversarial perturbations for robust face recognition. *International Journal of Computer Vision*, 2019.
- [34] Rui Shao, Pramuditha Perera, Pong C. Yuen, and Vishal M. Patel. Open-set adversarial defense with clean-adversarial mutual learning. *International Journal of Computer Vision*, 2022.
- [35] Aishan Liu, Xianglong Liu, Chongzhi Zhang, Hang Yu, Qiang Liu, and Dacheng Tao. Training robust deep neural networks via adversarial noise propagation. *IEEE Transactions on Image Processing*, 2021.
- [36] Lukas Schott, Jonas Rauber, Matthias Bethge, and Wieland Brendel. Towards the first adversarially robust neural network model on mnist. In *International Conference on Learning Representations*, 2019.
- [37] Francesco Croce and Matthias Hein. Provable robustness against all adversarial ℓ_p -perturbations for $p \geq 1$. In *International Conference on Learning Representations*, 2020.
- [38] Cassidy Laidlaw, Sahil Singla, and Soheil Feizi. Perceptual adversarial robustness: Defense against unseen threat models. In *International Conference on Learning Representations*, 2021.
- [39] Wei-An Lin, Chun Pong Lau, Alexander Levine, Rama Chellappa, and Soheil Feizi. Dual manifold adversarial robustness: Defense against ℓ_p and non- ℓ_p adversarial attacks. In *Advances in Neural Information Processing Systems*, 2020.
- [40] Pratyush Maini, Xinyun Chen, Bo Li, and Dawn Song. Perturbation type categorization for multiple ℓ_p bounded adversarial robustness. 2020.
- [41] Sergey Ioffe and Christian Szegedy. Batch normalization: Accelerating deep network training

- by reducing internal covariate shift. In *International Conference on Machine Learning*, 2015.
- [42] Xun Huang and Serge Belongie. Arbitrary style transfer in real-time with adaptive instance normalization. In *IEEE International Conference on Computer Vision*, 2017.
- [43] Yanghao Li, Naiyan Wang, Jianping Shi, Jiaying Liu, and Xiaodi Hou. Revisiting batch normalization for practical domain adaptation. In *International Conference on Learning Representations*, 2017.
- [44] Woong-Gi Chang, Tackgeun You, Seonguk Seo, Suha Kwak, and Bohyung Han. Domain-specific batch normalization for unsupervised domain adaptation. In *IEEE Conference on Computer Vision and Pattern Recognition*, 2019.
- [45] Lucas Deecke, Iain Murray, and Hakan Bilen. Mode normalization. In *International Conference on Learning Representations*, 2019.
- [46] Lei Huang, Jie Qin, Yi Zhou, Fan Zhu, Li Liu, and Ling Shao. Normalization techniques in training dnns: Methodology, analysis and application. *arXiv preprint arXiv:2009.12836*, 2020.
- [47] Harm de Vries, Florian Strub, Jeremie Mary, Hugo Larochelle, Olivier Pietquin, and Aaron C Courville. In *Advances in Neural Information Processing Systems*, 2017.
- [48] Bailin Li, Bowen Wu, Jiang Su, and Guangrun Wang. Eagleeye: Fast sub-net evaluation for efficient neural network pruning. In *ECCV*, 2020.
- [49] Philipp Benz, Chaoning Zhang, Adil Karjauv, and In So Kweon. Revisiting batch normalization for improving corruption robustness. In *WACV*, 2021.
- [50] Jan Hendrik Metzen, Volker Fischer, and Bastian Bischoff. On detecting adversarial perturbations. In *International Conference on Learning Representations*, 2018.
- [51] Cihang Xie and Alan Yuille. Intriguing properties of adversarial training at scale. In *International Conference on Learning Representations*, 2020.
- [52] Cihang Xie, Mingxing Tan, Boqing Gong, Jiang Wang, Alan L Yuille, and Quoc V Le. Adversarial examples improve image recognition. In *IEEE Conference on Computer Vision and Pattern Recognition*, 2020.
- [53] Yann LeCun. The mnist database of handwritten digits. <http://yann.lecun.com/exdb/mnist/>, 1998.
- [54] Alex Krizhevsky and Geoffrey Hinton. Learning multiple layers of features from tiny images. Technical report, Citeseer, 2009.
- [55] Jiayu Wu, Qixiang Zhang, and Guoxi Xu. Tiny imagenet challenge. 2017.
- [56] Yann LeCun, Léon Bottou, Yoshua Bengio, and Patrick Haffner. Gradient-based learning applied to document recognition. *Proceedings of the IEEE*, 1998.
- [57] Kaiming He, Xiangyu Zhang, Shaoqing Ren, and Jian Sun. Deep residual learning for image recognition. In *IEEE Conference on Computer Vision and Pattern Recognition*, 2016.
- [58] Karen Simonyan and Andrew Zisserman. Very deep convolutional networks for large-scale image recognition. *International Conference on Learning Representations*, 2015.
- [59] Sergey Zagoruyko and Nikos Komodakis. Wide residual networks. In *The British Machine Vision Conference*, 2016.
- [60] Wieland Brendel, Jonas Rauber, Matthias Kümmeler, Ivan Ustyuzhaninov, and Matthias Bethge. Accurate, reliable and fast robustness evaluation. In *Advances in Neural Information Processing Systems*, 2019.
- [61] Nicholas Carlini and David Wagner. Towards evaluating the robustness of neural networks. In *IEEE Symposium on Security and Privacy*, 2017.
- [62] Jonas Rauber, Wieland Brendel, and Matthias Bethge. Foolbox: A python toolbox to benchmark the robustness of machine learning models. 2017.
- [63] Wieland Brendel, Jonas Rauber, and Matthias Bethge. Decision-based adversarial attacks:

- Reliable attacks against black-box machine learning models. In *International Conference on Learning Representations*, 2018.
- [64] Francesco Croce and Matthias Hein. Reliable evaluation of adversarial robustness with an ensemble of diverse parameter-free attacks. In *International Conference on Machine Learning*, 2020.
- [65] Hongyang Zhang, Yaodong Yu, Jiantao Jiao, Eric P Xing, Laurent El Ghaoui, and Michael I Jordan. Theoretically principled trade-off between robustness and accuracy. 2019.
- [66] Dimitris Tsipras, Shibani Santurkar, Logan Engstrom, Alexander Turner, and Aleksander Madry. Robustness may be at odds with accuracy. In *International Conference on Learning Representations*, 2019.
- [67] Anish Athalye, Nicholas Carlini, and David Wagner. Obfuscated gradients give a false sense of security: Circumventing defenses to adversarial examples. *International Conference on Machine Learning*, 2018.
- [68] Yuki M Asano, Christian Rupprecht, and Andrea Vedaldi. A critical analysis of self-supervision, or what we can learn from a single image. In *International Conference on Learning Representations*, 2020.
- [69] Shiyu Tang, Ruihao Gong, Yan Wang, Aishan Liu, Jiakai Wang, Xinyun Chen, Fengwei Yu, Xianglong Liu, Dawn Song, Alan Yuille, Philip H.S. Torr, and Dacheng Tao. Robuststart: Benchmarking robustness on architecture design and training techniques. <https://arxiv.org/pdf/2109.05211.pdf>, 2021.
- [70] Dong Yin, Gontijo Raphael Lopes, Jonathon Shlens, D Ekin Cubuk, and Justin Gilmer. A fourier perspective on model robustness in computer vision. In *Advances in Neural Information Processing Systems*, 2019.
- [71] Van Laurens, Maaten Der, and Geoffrey Hinton. Visualizing data using t-sne. *Journal of Machine Learning Research*, 2008.
- [72] Yuxin Wu and Kaiming He. Group normalization. In *European Conference on Computer Vision*, 2018.
- [73] Dmitry Ulyanov, Andrea Vedaldi, and Victor S. Lempitsky. Instance normalization: The missing ingredient for fast stylization. *arXiv preprint arXiv:1607.08022*, 2016.
- [74] Jimmy Lei Ba, Jamie Ryan Kiros, and Geoffrey E Hinton. Layer normalization. *arXiv preprint arXiv:1607.06450*, 2016.
- [75] Alexey Dosovitskiy, Lucas Beyer, Alexander Kolesnikov, Dirk Weissenborn, Xiaohua Zhai, Thomas Unterthiner, Mostafa Dehghani, Matthias Minderer, Georg Heigold, Sylvain Gelly, et al. An image is worth 16x16 words: Transformers for image recognition at scale. In *International Conference on Learning Representations*, 2020.